Catalysis Today 427 (2024) 114409

Contents lists available at ScienceDirect

Catalysis Today

journal homepage: www.elsevier.com/locate/cattod

New scaling relationships for the oxygen evolution reaction on single atom catalysts

Ilaria Barlocco, Giovanni Di Liberto [*,1], Gianfranco Pacchioni

Dipartimento di Scienza dei Materiali, Università Degli Studi di Milano Bicocca, Via R. Cozzi 55, 20125 Milano, Italy

ARTICLE INFO

Keywords:
DFT
SAC
Scaling relations
OER
Intermediates

ABSTRACT

Single atom catalysis is relatively new frontier in catalysis with potential application in several critical chemical processes, such as water splitting reactions. Single atom catalysts (SACs) are analogues of coordination chemistry compounds, opening the way to the formation of unconventional intermediates compared to extended metal or oxide catalyst surfaces. In this work we show by means of density functional theory (DFT) calculations that the formation of unconventional adsorbates on SACs in the oxygen evolution reaction (OER) leads to complex scaling relationships, that differ from the scaling relations observed on extended surfaces. The evidence of new scaling relations directly impacts the expected catalytic activity and provides a further example of the importance of including in the modelling species beyond those that form on classical electrodes.

1. Introduction

Single Atom Catalysis is a relatively new frontier in the field of catalysis over the last decade [1–3]. A Single Atom Catalyst (SAC) is a paradigm of single-site catalysts being made by a transition metal atom dispersed in a matrix [4,5]. The quest for reducing the need of critical raw materials and improving the activity of existing catalysts is boosting the attention toward these systems. Indeed, SACs are potential candidates to overcome these problems. A very intense research is dedicated to critical reactions such as water splitting, nitrogen fixation, CO_2 electro-reduction, synthesis of chemicals etc. [6–11].

The activity of SACs can be tailored, ideally designed, by engineering the local coordination of the metal atoms with atomic precision [10,12,13]. In addition, SACs share some analogies with coordination chemistry compounds [12]. This evidence manifests itself in a rich and complex chemistry, opening potential ways to optimize the catalytic activity. These two aspects make the fundamental understanding of the nature and reactivity of SACs challenging. Experimental techniques with atomic precision and computational studies are therefore powerful and somewhat essential tools in this respect [13–17].

Computational studies can model at the quantum mechanical level the structure of SACs, their properties and reactivity, eventually providing a fundamental rationale. In the last years theory is trying to address the more ambitious purpose of predicting new potential systems by taking advantage of general descriptors [18–21]. This goal is motivated by both the success in the field of heterogeneous catalysis and the increase of computational power.

Descriptors are key-properties, often thermodynamic variables, allowing to predict the catalytic activity of a specific system [22,23]. Two paradigmatic examples are the hydrogen evolution (HER) and the oxygen evolution (OER) reactions, the two sides of water splitting. Some time ago Norskov and co-workers proposed seminal works demonstrating that both reactions can be described by the thermodynamic stability of specific reaction intermediates [24–28]. In particular, universality was found in OER on extended catalysts made by metals and oxides [29]. More specifically, it was demonstrated that the thermodynamic stability of reactions intermediates scales linearly with the formation energy of the first intermediate. OER is assumed to pass through the following four mono-electronic steps and consequent formation of OH*, O*, OOH* intermediates [26].

$$* + H_2O \rightarrow OH* + H^+ + e^- \quad (1)$$

$$OH* \rightarrow O* + H^+ + e^- \quad (2)$$

$$O* + H_2O \rightarrow OOH* + H^+ + e^- \quad (3)$$

$$OOH* \rightarrow O_2 + H^+ + e^- \quad (4)$$

It is known that the reaction is limited by a finite overpotential

* Correspondence to: Università Milano-Bicocca, Dipartimento di Scienza dei Materiali, Via R. Cozzi 55, 20125 Milano, Italy.
E-mail address: giovanni.diliberto@unimib.it (G. Di Liberto).
[1] ORCID: 0000-0003-4289-2732.

https://doi.org/10.1016/j.cattod.2023.114409
Received 24 July 2023; Received in revised form 27 September 2023; Accepted 11 October 2023
Available online 14 October 2023

described by a volcano curve with a minimum value of about 0.4 eV [25]. This evidence is appointed to the existence of scaling relations between the intermediates, and in particular to the following one: $\Delta G_{OOH^*} = \Delta G_{OH^*} + 3.2$ eV [30]. The minimum overpotential is obtained when the energy difference x between OH* and O* (and consequently of OOH*) corresponds to $x = \Delta G_{O^*} - \Delta G_{OH^*} = 1.6$ eV [31].

Typically, the reactivity of SACs is assumed to be the same as for classical heterogeneous catalysts, and therefore the mentioned descriptors are used to provide predictions or perform screenings studies aimed to discover new SACs. However, SACs can form other unconventional intermediates, as recently demonstrated for both the HER and OER processes. For instance, once an OH* species forms, another water molecule can be adsorbed forming a OH*OH* intermediate, that can compete in stability with O* [32,33]. In our nomenclature the unconventional species, as OH*OH*, are bound to the same catalytic site, and therefore it should be labelled as (OHOH)*. However, we prefer to adopt the first version to underline that each adsorbate is directly bound to the active site.

$$OH^* + H_2O \rightarrow OH^*OH^* + H^+ + e^- \quad (5)$$

Similarly, the OH*O* intermediate competes with the OOH* one [33].

$$O^* + H_2O \rightarrow OOH^* + H^+ + e^- \quad (6a)$$

or.

$$O^* + H_2O \rightarrow OH^*O^* + H^+ + e^- \quad (6b)$$

Eventually, before molecular oxygen release occurs, another stable oxygen complex can form:

$$OOH^* + H_2O \rightarrow O_2 + H^+ + e^- \quad (7a)$$

or.

$$OH^*O^* \rightarrow O_2 + H^+ + e^- \quad (7b)$$

Clearly, neglecting these species from the study of the reaction profile can have serious impact on the definition of the reaction mechanism and of its kinetics. Moreover, some reports showed that for specific adsorbates and SACs linear scaling relations can be broken [32,34,35].

In this work we show that the inclusion of unconventional intermediates for the OER leads to scaling relations that differ

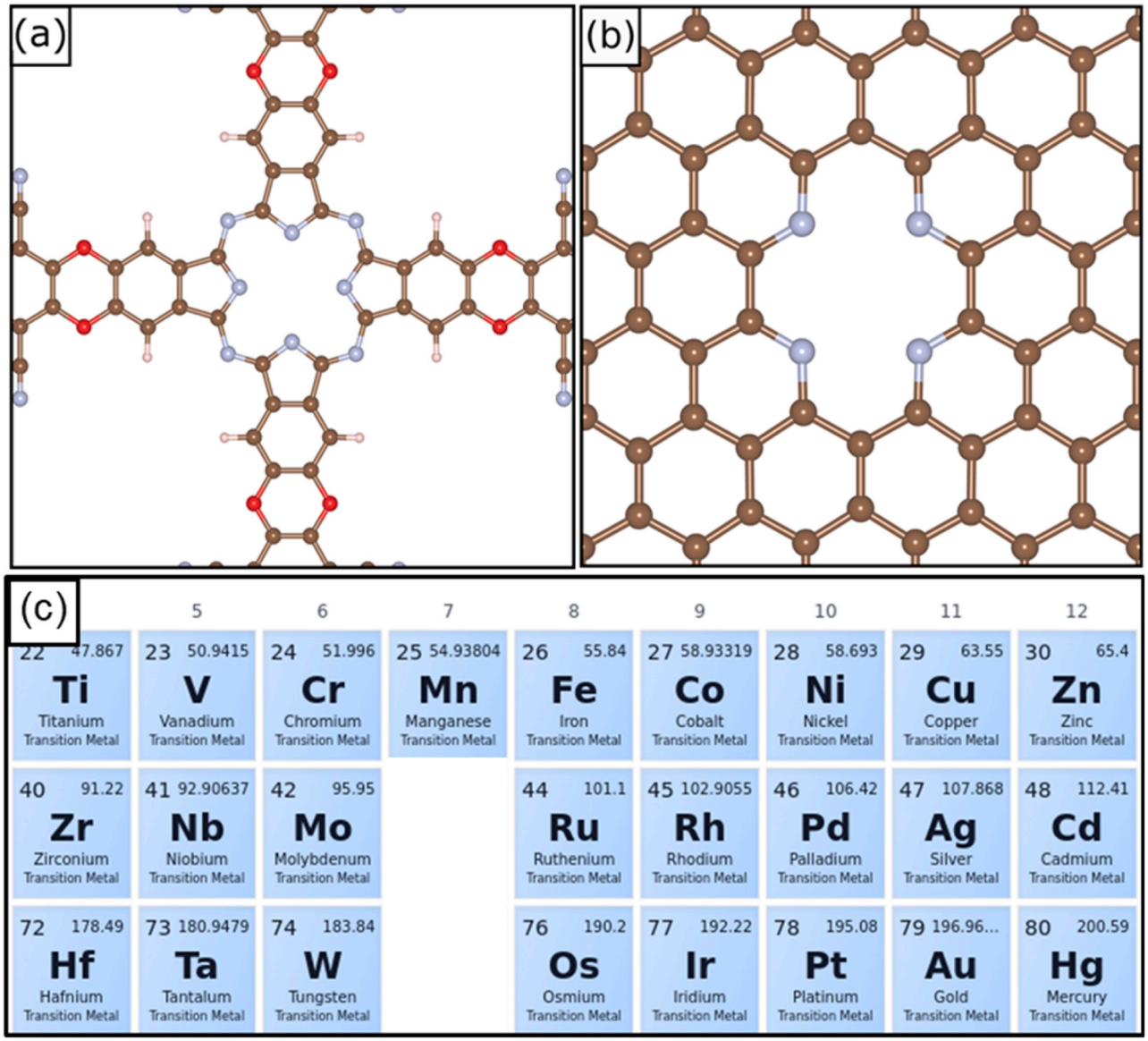

Fig. 1. Structure of the available cavities of COF (a) and 4 N-Gr (b). (c) reports the transition metal atoms studied in this work.

substantially from the classical ones derived for standard heterogeneous catalysts. This evidence directly impacts the predictions of optimal SACs for OER.

We studied a data set of 25 transition metal atoms (reported in Fig. 1; Sc and Re were not included since we encountered convergence problems, while Tc is radioactive and unstable) embedded in two carbonaceous matrices for a total of 50 SACs. The selected supports are nitrogen-doped graphene (4 N-Gr) and a covalent organic framework obtained through the combination of metallophthalocyanine and pyrazine (COF). The first one is widely adopted as a template and the latter is emerging has a suitable support due to its capability to strongly bind metal atoms [36]. Given the large number of calculations involved, we restrict our study to a standard level of electronic structure description, i.e. density functional theory (DFT) with correction of the self-interaction error according to the DFT+*U* approach.

The main result of this work is that the minimum overpotential predicted from this analysis is slightly lower than the same quantity derived for heterogeneous catalysts (0.4 eV). This means that it is possible, at least in principle, to find catalysts based on single sites that can be more active than the classical extended catalytic surfaces. Furthermore, the search for scaling relationships allows one to predict what kind of intermediate will be formed as function of a specific descriptor, a fundamental starting point for screenings of the catalytic activity of unknown systems. This work also highlights the importance of extending the computational framework to species that on conventional catalysts would not form. Finally, it must be underlined that the purpose of the study is not to reproduce the experimental complexity or to predict new catalysts, but only to provide some general rules.

2. Computational details

We performed DFT calculations by means of the VASP package (version 6.2) [37–39]. The Perdew-Burke-Ernzherof (PBE) parameterization has been used for the exchange-correlation functional [40]. The valence electrons were expanded on a set of plane waves with a kinetic cutoff of 400 eV. Core electrons were treated with Projector Augmented Wave (PAW) pseudopotentials [41,42]. The following valence electrons were treated explicitly: H (1 s), C (2 s, 2p), N (2 s, 2p), O (2 s, 2p), Ti (3 s, 3p, 4 s, 3d), V (3 s, 3p, 4 s, 3d), Cr (3p, 4 s, 3d), Mn (3p, 4 s, 3d), Fe (4 s, 3d), Co (4 s, 3d), Ni (4 s, 3d), Cu (4 s, 3d), Zn (4 s, 3d), Zr (4 s, 4p, 5 s, 4d), Nb (4p, 5 s, 4d), Mo (4p, 5 s, 4d), Ru (4p, 5 s, 4d), Rh (4p, 5 s, 4d), Pd (5 s, 4d), Ag (5 s, 4d), Cd (5 s, 4d), Hf (5p, 6 s, 5d), Ta (5p, 6 s, 5d), W (5p, 6 s, 5d), Os (6 s, 5d), Ir (6 s, 5d), Pt (6 s, 5d), Au (6 s, 5d), Hg (6 s, 5d). Dispersion forces have been included by the Grimme's D3 scheme [43]. The convergence criteria of electronic and ionic loops were 10^{-5} eV and 10^{-2} eV/Å respectively. The Conjugate Gradient algorithm was adopted to search of minimum energy structures. The sampling of the reciprocal space was adapted to provide converged results. More specifically, a $4 \times 4 \times 1$ Monkhorst−Pack k-point grid was used to sample the reciprocal space when working with 4 N-Gr support, while for COFs, the sampling was reduced to the gamma point because of the large cell size. Each structure, either SAC or adsorbed species was obtained upon geometry optimization of the atomic coordinates. PBE is a widespread and efficient functional but it has limitations to describe systems with a certain degree of electron localization. A possible way to improve the picture is to adopt hybrid functionals. For instance, a previous study suggested that PBE0 or HSE06 calculations are sufficient to reproduce benchmark calculations beyond DFT of hydrogen adsorption on a SAC taken as test case [44]. However, hybrid functional calculations are computationally demanding. A possible trade-off is represented by the DFT+*U* approach. In this case, a correction term is added to the functional to account for the self-interaction error. Table 1 reports the *U* parameters used in this work for the atoms of interest. They have been already tested in previous studies, including a discussion of their origin [45]. PBE+*U* calculated quantities are in much better agreement with the PBE0 hybrid functional that with the semi-local PBE one [46].

Table 1
Adsorption energy, atomic magnetization, and M-N bond distances of TMs adsorbed in the cavity of COF and 4 N-Gr. The *U* parameter used in the calculations is also reported.

Catalyst	E_{ad} /eV	μ_B	dM-N /Å	*U* /eV
Ti@COF	-10.46	1.05	2.02	2.58
V@COF	-10.13	2.37	2.01	2.72
Cr@COF	-9.36	3.55	2.00	2.93
Mn@COF	-8.24	3.44	1.98	3.06
			1.96	
Fe@COF	-8.93	2.02	1.96	3.29
Co@COF	-9.27	1.05	1.95	3.42
Ni@COF	-9.46	0.00	1.94	3.40
Cu@COF	-7.74	0.61	1.97	4.20
Zn@COF	-6.80	0.00	1.99	4.40
Zr@COF	-11.20	0.53	2.14	1.76
Nb@COF	-11.12	1.28	2.04	2.02
Mo@COF	-9.27	2.86	2.05	2.30
Ru@COF	-9.51	1.66	2.01	2.79
Rh@COF	-9.26	0.90	2.01	3.04
Pd@COF	-8.39	0.00	1.99	3.33
Ag@COF	-5.33	0.46	2.05	3.60
Cd@COF	-4.60	0.00	2.08	3.80
Hf@COF	-11.52	0.50	2.11	1.65
			2.12	
Ta@COF	-11.98	1.04	2.03	1.87
W@COF	-11.17	2.33	2.03	2.08
Os@COF	-9.98	1.54	2.00	2.51
Ir@COF	-10.34	0.73	1.99	2.74
Pt@COF	-10.58	0.00	1.99	2.95
Au@COF	-5.91	0.01	2.01	3.20
Hg@COF	-2.10	0.00	2.11	3.40
Ti@4 N-GR	-7.41	1.06	2.08	2.58
			2.00	
V@4 N-GR	-7.03	2.40	2.00	2.72
Cr@4 N-GR	-6.22	3.57	1.96	2.93
Mn@4 N-GR	-5.41	3.29	1.93	3.06
Fe@4 N-GR	-6.26	2.02	1.92	3.29
Co@4 N-GR	-6.67	1.03	1.90	3.42
Ni@4 N-GR	-7.07	0.00	1.89	3.40
Cu@4 N-GR	-5.17	0.57	1.93	4.20
Zn@4 N-GR	-4.05	0.00	1.94	4.40
Zr@4 N-GR	-8.35	0.40	2.13	1.76
Nb@4 N-GR	-1.79	0.96	1.99	2.02
Mo@4 N-GR	-5.28	2.98	1.99	2.30
Ru@4 N-GR	-6.14	1.63	1.96	2.79
Rh@4 N-GR	-6.15	0.68	1.95	3.04
Pd@4 N-GR	-5.43	0.00	1.95	3.33
Ag@4 N-GR	-2.13	0.40	2.00	3.60
Cd@4 N-GR	-0.99	0.00	2.03	3.80
Hf@4 N-GR	-8.59	0.43	2.11	1.65
Ta@4 N-GR	-8.58	0.85	2.11	1.87
			2.00	
W@4 N-GR	-7.31	1.96	2.02	2.08
Os@4 N-GR	-6.30	1.93	1.97	2.51
Ir@4 N-GR	-7.17	0.73	1.95	2.74
Pt@4 N-GR	-7.40	0.00	1.95	2.95
Au@4 N-GR	-2.94	0.00	1.96	3.20
Hg@4 N-GR	-0.31	0.00	3.18	3.40

We adsorbed 25 TM atoms on two different supports, nitrogen-doped graphene (4 N-Gr) and a covalent organic framework (COF). 4 N-Gr is a typical support for SACs [47–49]. COFs are emerging as good templates for SACs because of their ability to strongly bind the metal atoms and thanks to the possibility to control the size and shape of the hosting cavities [50–52]. Fig. 1 shows the local structure of the available cavities. They are similar to the bonding environment of metal-porphyrins, largely used in homogeneous catalysts. The 4 N-Gr model was generated by fully optimizing a graphene nanosheet, creating a carbon-divacancy, and replacing four carbon atoms with nitrogen (4 N-Gr). The atomic coordinates of the resulting structure have been fully reoptimized. This kind of cavity is a common anchoring site for SACs. In the case of COFs, we considered a recently established framework [51]. The structural parameters of both models are reported in Table S1.

The stability of the reaction intermediates was calculated by adopting the classical thermodynamic approach [24,26]. The Gibbs free energy was estimated as:

$$\Delta G = \Delta E - T\Delta S + \Delta E_{ZPE} \quad (8)$$

where ΔE is the calculated DFT energy, $T\Delta S$ is the entropic contribution and ΔE_{ZPE} is the zero-point energy correction. In each case we let vibrate the atoms of the intermediate and the metal single atom [33,53]. $T\Delta S$ of solid-state species was neglected, and that of gas-phase molecules was taken from International Tables. This approximation can be improved by evaluating vibrational entropy from the partition function. Since the scope of the study is not to provide absolute predictions, we restrict to the inclusion of the entropy of gas-phase species only. The zero-point energy of the species were determined in a harmonic fashion allowing to vibrate the metal atoms and those of the adsorbed intermediates. Tables S2 and S3 report the related quantities. Last, it is well known that DFT has issues in reproducing the O-O binding energy [54]. A typical way to tame this problem is to use the experimental energy for OER (4.92 eV) [26]. We also mention that other approaches have been proposed recently to face this problem [55].

3. Results and discussion

3.1. Intermediates of OER on SACs

Fig. S1 shows some examples of atomic structure of each catalyst consisting of one of the 25 TM atoms anchored to the two supports. Table 1 reports some key properties such as relevant bond distances, adhesion energy and atomic magnetization. One can see that both supports strongly bind the TM atoms, but on average COF binds stronger than 4 N-Gr [56]. Also, the metal atoms often display some residual atomic magnetization, typical of the atomic like character of several SACs [57].

These catalysts show similarities with their organometallic counterparts, in particular with porphyrins. As an example, R. J. Needs and co-workers [58] investigated metal porphyrin (with M= Ni, Cu, Zn) by using Quantum Monte Carlo method. The M-N distances were found to be 1.96 Å for Ni, 2.01 Å for Cu and 2.04 Å for Zn. The local structure of our SACs well compares with the molecular data; on COF we obtained the following values, 1.94 Å (Ni), 1.97 Å (Cu) and 1.99 Å (Zn). On 4 N-Gr the calculated distances are 1.89 Å (Ni), 1.93 Å (Cu) and 1.94 Å (Zn). Moreover, in further recent study, a Pt based porphyrin was synthesised and characterized by single crystal X-Ray diffraction founding a M-N bond length of about 2.01–2.02 Å [59]. Our calculated Pt-N distances compare well, 1.99 Å (COF) and 1.95 Å (4 N-Gr).

We used these catalysts to simulate the OER by computing the formation energy of various intermediates. We first considered the three classical OH*, O*, and OOH* species that are assumed to form in the course of the reaction. Then, we included also the OH*OH* and OH*O* intermediates, since it has been shown that SACs can bind the two adsorbates on the same side as well as on opposite sides of the single layer catalyst [33]. However, if the intermediates form on the opposite sides of the catalyst this result in high barriers for the OER and catalyst poisoning since diffusion of the intermediates on the same side is required for the reaction to occur.

The oxygen complexes were modelled by considering the formation of both superoxo and peroxo complexes. These are characterized by a different elongation of the O-O bond length, 1.25–1.35 Å superoxo, 1.35–1.45 Å peroxo [53,60,61]. We finally considered dioxo complexes where the O-O bond is completely broken resulting in large O-O distances [62,63]. The Gibbs free energy profiles reported in Fig. S2 were obtained by neglecting any reaction barriers different from those of thermochemistry according to Norskov approach [24,26,64]. The preferred reaction path is defined by the most stable reaction

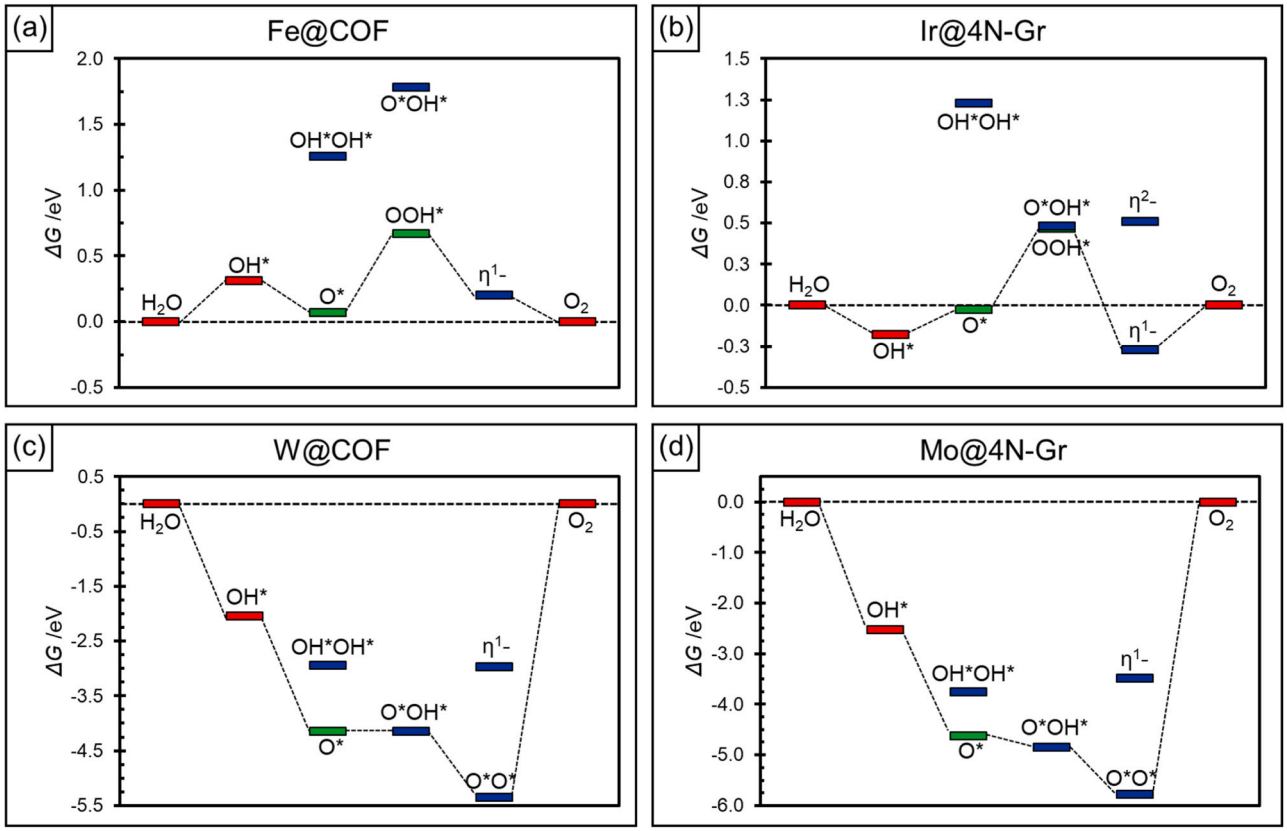

Fig. 2. Selected example of Gibbs free energy profile of Fe@COF, Ir@4 N-Gr, W@COF and Mo@4 N-Gr. The conventional and unconventional intermediates are represented in green and blue, respectively. In red the intermediates common to both pathways are showed.

intermediates. .

We notice that in 37 cases out of the total (50) the most stable path includes the presence of at least one unconventional intermediate, providing strong evidence of the importance of going beyond the classical OH* /O* /OOH* path when modelling OER on SACs. Table 2 reports all the calculated Gibbs free energies. Fig. 3 reports some selected examples of Gibbs free energy profiles of two SACs based on 4 N-Gr and two on COFs. In particular, the profile of W@COF and Mo@4 N-Gr shows that the SACs bind the intermediates too strongly, leading to very high barriers, while Fe@COF and Ir@4 N-Gr lead to profiles with much smaller barriers and the formation of a superoxo complex.

While the importance of accounting for unconventional intermediates is clear, it is not obvious to rationalize a priori when a specific intermediate is stable or not. The picture is very complex. There are cases such as Mo@COF, W@COF, Mo@4 N-Gr and W@4 N-Gr where the OH* O* intermediate is more stable than the OOH* one, and others (Rh@COF, Fe@COF and Co@COF and Rh@4 N-Gr and Ir@4 N-Gr) where the opposite is true. In some SACs, a dioxo complex forms (Mo and W on both supports); in some other a superoxo complex is more stable (Rh@ both 4 N-Gr and COF). Clearly, the rationalization of the results is hard without finding a suitable descriptor. Furthermore, the calculated overpotential (η) does not follow any simple general rule. There are SACs that appear promising for OER with small η, between 0.49 eV and 0.60 eV (Ir@4 N-Gr, Co@COF, Rh@4 N-Gr, Fe@COF and Rh@COF). Conversely, W@COF, Mo@COF, Mo@4 N-Gr and W@4 N-Gr overbind some species and therefore are predicted to be inactive catalysts, Table 2.

4. Scaling relations

In this section we discuss the possibility to gain understanding on the stability of OER intermediates on SACs based on the analysis of scaling relations. Scaling relations are correlations (often linear) that allow one to predict the free energies of all the remaining reaction intermediates in the catalytic cycle. They allow to reduce the complexity of the problem to the determination the activity of a few or even a single species, while the others are deduced from the scaling relations. Fig. 3 shows that the formation free energy of the O* and OH*OH* intermediates scale

Table 2
Calculated Gibbs free energy of various OER steps on TMs adsorbed in the cavity of COF and 4 N-Gr.

Catalyst	ΔG_{OH} /eV	ΔG_{O} /eV	ΔG_{OOH} /eV	ΔG_{OHOH} /eV	ΔG_{OHO} /eV	$\Delta G\eta^{1}$ /eV	$\Delta G\eta^{2}$ /eV	ΔG_{OO} /eV
Ti@COF	-1.51	-1.46	/	-1.02	0.81	1.27	1.25	/
V@COF	-0.60	-0.76	/	0.86	1.47	/	/	/
Cr@COF	1.62	1.89	4.88	3.11	4.46	4.53	4.87	/
Mn@COF	1.27	2.15	4.96	3.16	4.96	4.71	4.76	/
Fe@COF	1.54	2.53	4.36	3.72	5.47	5.12	/	/
Co@COF	1.70	3.44	4.75	5.00	6.65	4.99	/	/
Ni@COF	2.40	4.60	5.45	/	/	/	/	/
Cu@COF	2.73	5.00	5.54	5.95	7.57	/	/	/
Zn@COF	2.12	4.57	4.98	4.85	/	/	/	/
Zr@COF	-2.37	-1.87	1.07	-2.66	-0.35	/	0.49	2.14
Nb@COF	-2.03	2.30	/	-1.78	-1.97	0.96	/	-0.02
Mo@COF	-0.05	-0.86	3.09	0.41	0.54	3.69	/	0.76
Ru@COF	0.62	1.31	3.79	2.91	4.29	4.38	/	5.73
Rh@COF	1.14	2.97	4.49	4.24	5.88	4.63	/	7.76
Pd@COF	2.73	4.94	/	/	/	/	/	/
Ag@COF	2.78	5.09	/	5.25	7.14	/	6.84	/
Cd@COF	1.61	4.09	4.59	4.61	6.32	/	/	/
Hf@COF	-2.60	-1.84	0.90	-2.76	-0.52	/	0.41	1.88
Ta@COF	-1.92	-2.28	/	-2.23	-2.08	0.46	/	-0.19
W@COF	-0.81	-1.68	/	-0.48	-0.45	1.95	/	-0.43
Os@COF	0.49	0.90	3.64	2.38	3.05	4.24	/	4.10
Ir@COF	1.04	2.16	4.38	3.79	5.20	4.61	/	6.83
Pt@COF	2.63	4.84	/	/	/	/	/	/
Au@COF	/	/	/	4.50	6.88	/	/	9.02
Hg@COF	1.44	3.96	4.59	4.32	6.29	/	/	/
Ti@4 N-GR	-1.95	-1.87	-0.64	-1.59	/	2.34	0.72	/
V@4 N-GR	-0.97	-1.29	0.31	0.02	0.67	2.91	2.08	/
Cr@4 N-GR	0.36	1.18	3.71	2.19	3.20	4.11	4.15	/
Mn@4 N-GR	1.02	1.86	3.89	2.02	3.73	4.19	4.03	/
Fe@4 N-GR	1.29	2.22	4.46	2.61	4.21	4.69	4.86	/
Co@4 N-GR	1.43	2.64	4.58	3.67	5.21	4.71	5.47	/
Ni@4 N-GR	2.16	3.98	5.07	/	/	/	/	/
Cu@4 N-GR	2.01	4.35	4.98	4.16	6.26	/	/	/
Zn@ 4 N-GR	0.94	3.49	4.27	3.47	4.14	4.73	/	6.76
Zr@4 N-GR	-2.52	-1.99	0.86	-2.89	-1.22	/	0.31	1.04
Nb@4 N-GR	-3.22	-3.51	/	-3.37	-3.46	-0.61	/	-1.88
Mo@4 N-GR	-1.29	-2.16	/	-1.29	-1.16	1.44	/	-0.86
Ru@4 N-GR	0.35	1.04	/	1.98	2.66	3.95	4.08	/
Rh@4 N-GR	0.94	2.68	4.03	3.59	4.72	4.47	5.37	/
Pd@4 N-GR	2.52	4.78	5.22	/	/	/	/	/
Ag@4 N-GR	1.30	3.50	4.27	3.05	5.15	4.91	/	4.62
Cd@4 N-GR	-0.44	2.11	2.95	1.61	2.85	3.49	/	5.41
Hf@4 N-GR	-2.70	-1.96	0.74	-3.02	-1.36	/	0.19	1.02
Ta@4 N-GR	-2.46	-2.86	/	-3.08	-2.98	-0.25	/	-1.45
W@4 N-GR	-1.64	-2.73	/	-2.15	-2.17	0.67	/	-1.74
Os@4 N-GR	0.11	0.39	/	1.20	1.40	3.62	3.55	/
Ir@4 N-GR	1.05	2.43	4.16	3.69	4.17	4.65	5.43	/
Pt@4 N-GR	2.49	4.57	5.26	/	/	/	/	/
Au@4 N-GR	2.19	3.94	4.93	3.03	5.03	4.86	/	7.34
Hg@4 N-GR	1.01	3.47	4.39	/	/	4.95	/	/

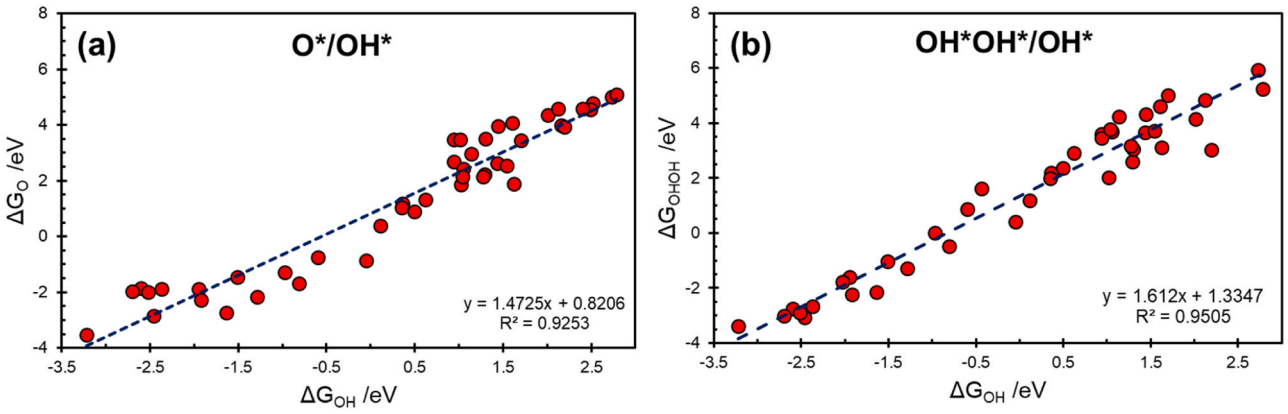

Fig. 3. Scaling relationship obtained comparing the mono- (OH*) and bi-electronic (O*, OH* OH*) steps of the OER.

linearly with that of the OH* species. Interestingly, the plot clearly indicates that the OH*OH* species is metastable with respect to O* . This becomes more evident when comparing the two correlation curves in Fig. S2. OH*OH* becomes more stable only when the catalyst binds OH* very strongly, i.e. $\Delta G_{OH^*} < -3.5$ eV. Of course, this energy window is not of catalytic interest since the intermediate is too stable and poisons the catalyst. Fig. 4 compares how the Gibbs free energies of formation of OOH* and OH*O* scale with that of OH* . In this case we see two possible solutions. When $\Delta G_{OH^*} < -0.5$ eV, the O*OH* species is preferred, while when the binding of OH* becomes weaker, OOH* becomes the most favourable intermediate, Fig. S3. This simple analysis allows one to predict which adsorbate will form looking at the stability of the first OER intermediate, i.e. the OH* species.

Fig. 5 reports a similar comparison. The Gibbs formation energy of the OH* intermediate is plotted against that of the last step in the reaction, where η^1 (superoxo), η^2 (peroxo), and O* O* (di-oxo) species can form. Fig. S4 compares the three correlation curves. When $\Delta G_{OH^*} < -0.75$ eV the most stable adsorbate is a di-oxo O*O* compound. As the interaction becomes weaker the superoxo configuration becomes favourable. All adducts are less stable than the separate O_2 molecule when $\Delta G_{OH^*} > 1.25$ eV. Superoxo and peroxo complexes are always nearly isoenergetic. We observe that the data are sparse for the O*O* case ($R^2 = 0.69$), probably because this adduct shows the largest structural changes when comparing different SACs.

Once the analytical functions describing the stability of all intermediates with respect to a specific one, OH* in this case, have been obtained, it is possible to calculate the reaction barriers assuming to work at a given applied voltage. Typically, barriers are evaluated at $V = 1.23$ V, corresponding to the ideal OER equilibrium potential. The highest barrier corresponds to the overpotential. We repeat that reaction barriers are evaluated solely considering the thermodynamic stability of the intermediates, not the transition states, a common approach.

For extended metal or oxide catalytic surfaces, the existence of linear relations makes it possible to calculate the reaction barriers of each monoelectronic step (*→OH*, OH*→O*, O*→OOH*, OOH*→O_2) as a function of a simple descriptor. The typical descriptor is taken as $x = \Delta G_{O^*} - \Delta G_{OH^*}$ [25]. For each value of x, the highest barrier defines the overpotential (if one assumes to work at $V = 1.23$ V). Based on the classical scaling relation $\Delta G_{OOH^*} = \Delta G_{OH^*} + 3.2$ eV [30], two electrons are needed to pass from OH* to OOH* ; the optimal condition corresponds into having an overpotential equal to (3.2 eV – 1.23 V*2e) / 2e = 0.37 V [30]. The potential corresponding to the minimum overpotential is 3.2 eV / 2e = 1.6 V [30]. The left hand of the volcano occurs when the limiting step is the desorption of O_2 from OOH, OOH* →O_2. The right branch is found when * →OH* is the limiting process.

We did a similar analysis on our database of SACs considering the formation of all intermediates discussed above. Fig. 6 shows the calculated overpotential based on the raw data (solid circles) and the same obtained from the analytical linear functions extrapolated from the correlations reported in Figs. 2–4. We have chosen a descriptor in Fig. 6 that can be considered as a generalization of the common one in conventional catalysts [25,65], i.e. $x = \Delta G_{O^*/OH^*OH^*} - \Delta G_{OH^*}$. We have seen above that the formation of unconventional intermediates leads to new scaling relations, and that they direct impact the shape of the Gibbs free energy profiles. These, in turn, affect that predicted overpotential. As expected, the increased number of intermediates and the emerging of new relations leads to a more complex shape of the volcano curve. Interestingly, if one restricts the analysis to the region close to the optimal conditions, i.e. minimum overpotential, the classical scaling relations works in an acceptable way. This can explain the reason why often classical scaling relations are used to solve problems of OER on SACs [66–68]. Nevertheless, if one considers a broader window, the

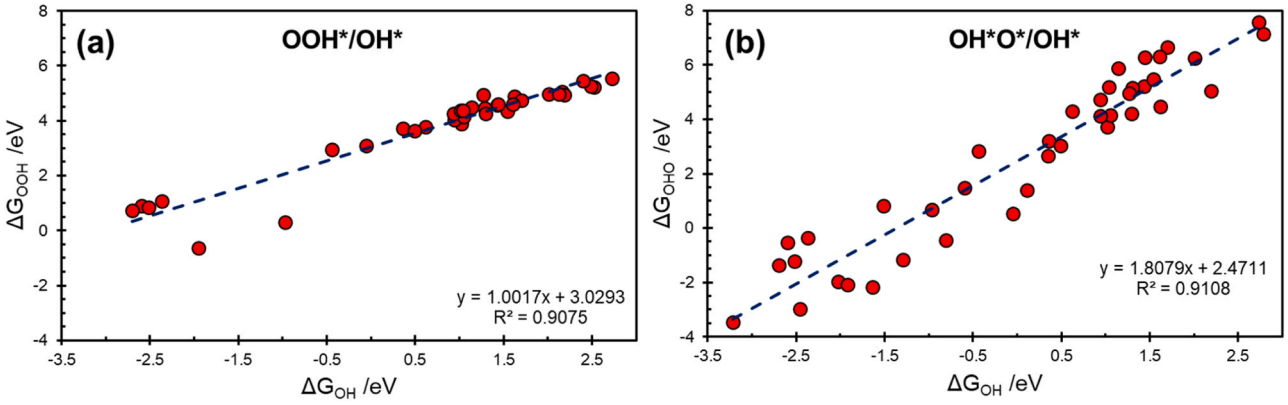

Fig. 4. Scaling relationship obtained comparing the mono- (OH*) and tri-electronic (OOH*, OH*O*) steps of the OER.

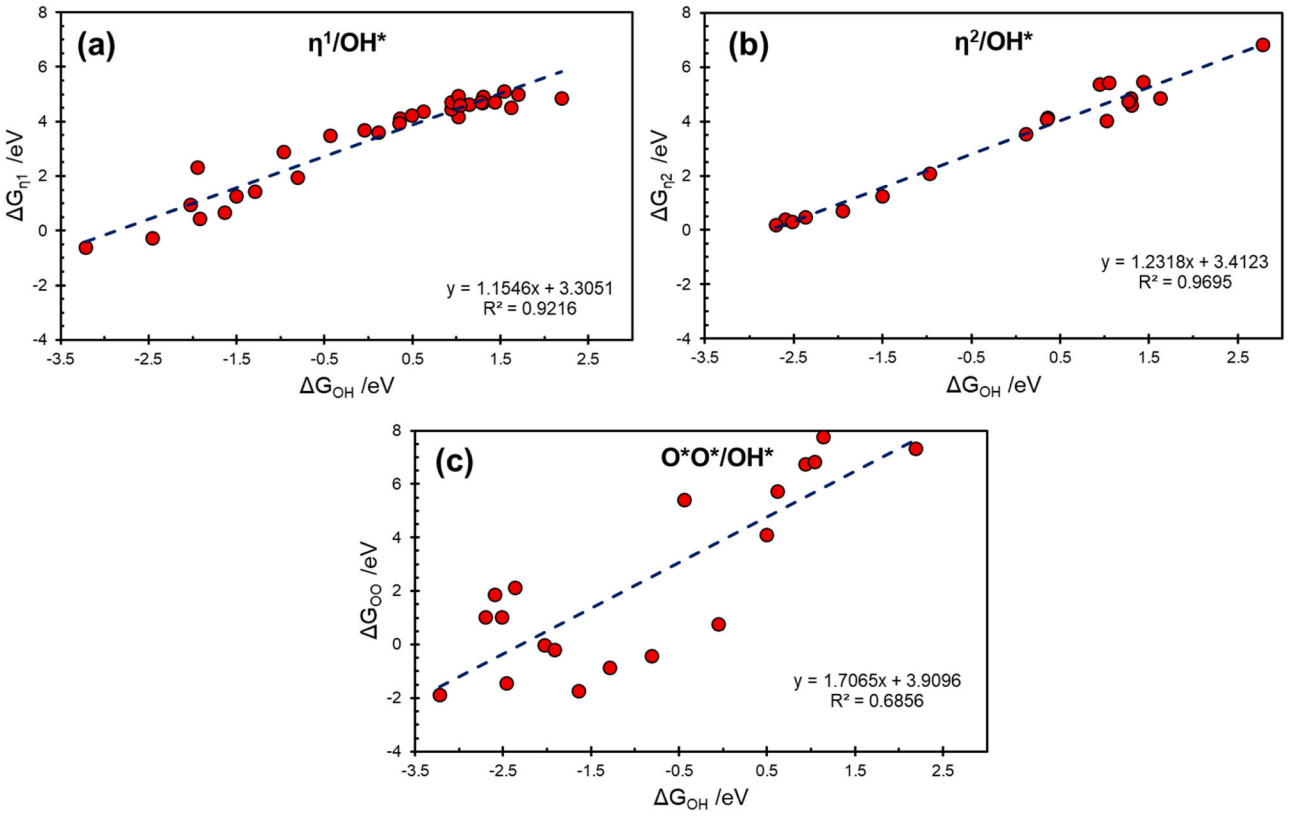

Fig. 5. Scaling relationship obtained comparing the monoelectronic step (OH*) and the oxygen complexes η^1 (superoxo), η^2 (peroxo), and O*O* (di-oxo) formed on single atom catalysts.

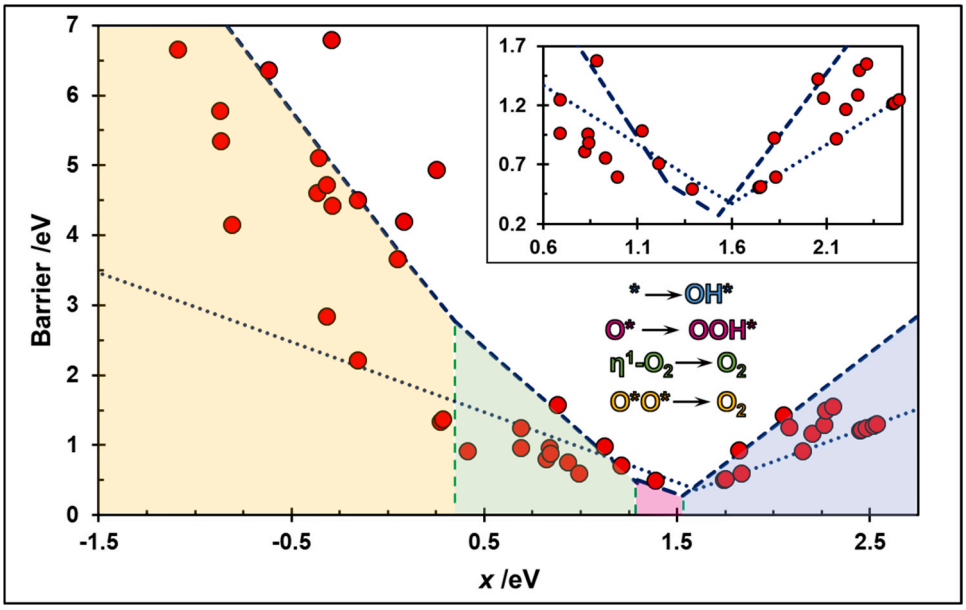

Fig. 6. Calculated overpotential based on the raw data (solid circles, see Table 2) and the same obtained from analytical functions extrapolated from the correlations found, see Fig. s 3–5 (dashed line). The results for any extended catalyst obtained by using universal scaling relations considering only the classical OH*, O*, OOH* species is reported with dotted lines. Different colors correspond to the formation of different intermediates. The inset shows an enlargement of the region corresponding to the apex of the volcano curve, which indicates the minimum overpotential required for the reaction.

picture changes dramatically. This is particularly evident by analysing the left branch of the plot, where several systems have a calculated overpotential considerably larger than that obtained from classical scaling relations. This is due to the fact that this part of the plot is characterized by a determining step consisting in the release of oxygen from a di-oxo complex, a species that is typically not considered. Interestingly, at $x = 0.35$ eV there is a change in the slope due to a change in the limiting process, from O*O* $\rightarrow O_2$ to η^1-$O_2 \rightarrow O_2$. We recall that in the classical scheme, the left branch of the plot is characterized by the release of oxygen from OOH* . This picture is retrieved only when

1.3 eV $< x <$ 1. 5 eV, and not surprisingly the slope of the curve is the same of the classical OOH* $\rightarrow O_2$ relation. The right branch of the plot shows a situation where the formation of OH* is the rate determining step of the reaction. The extrapolation of the minimum value corresponds to $x = 1.5$ eV, which is not too different from the minimum value that one obtains from scaling relations of the extended catalysts (1.6 eV). This small reduction of x results in a reduction of the minimum overpotential to about 0.2 eV, i.e. 0.2 eV lower that the generally accepted value of 0.4 of eV of classical electrocatalysts.

It must be mentioned that some numerical differences could originate from the inherent approximations adopted. At the same time, the emerging of new scaling relations is clear, and it is mainly due to the formation of unconventional intermediates, with the consequence that for some catalysts the expected catalytic activity can be higher. The results also show that the chemistry of SACs is rather rich and that it is important to include the formation all intermediates if one wants to describe the reaction profile. We have also seen that changes to the nature of the limiting step of the reaction leads to linear curves with different slopes, defining specific branches of the volcano. Therefore, all unconventional intermediates must be included when treating OER on SACs, since neglecting some species can affect the predictions.

Further work will be dedicated in future studies to investigate *i)* the role of the computational setup, and in particular of hybrid functionals, *ii)* the generality of the message to other relevant supports beside N-doped graphene and COFs.

5. Conclusions

In this work we performed a computational study of the Oxygen Evolution Reaction on a set of 50 Single Atom Catalysts, consisting of 25 transition metal atoms embedded in two supports, nitrogen-doped graphene and a covalent organic framework. Based on the calculated stability of both classical (OH*, O*, OOH*) and unconventional (OH*OH*, O*OH*, η^1-O_2 *, η^2-O_2 *, and O*O*) intermediates we have found a set of linear scaling relations. As a simple descriptor we used the Gibbs formation energy of the first species that forms in OER, OH*. This allows one to indirectly predict stable adsorbates even without performing explicit DFT calculations. Importantly, we found that the formation of unconventional intermediates leads to classical relations different from those known for extended heterogeneous catalysts. This results into a different shape of the volcano overpotential curve, associated with a small reduction of the optimal overpotential by about 0.2 eV from the classically accepted value of 0.4 eV.

These results not only demonstrate once more the importance of including unconventional intermediates in the modelling of OER on SACs, but they suggest that it is possible to improve the catalytic activity thanks to the rich chemistry of SACs. Future studies will be devoted to establish the role of more demanding computational frameworks to improve the accuracy of the calculated Gibbs free energies and to investigate the generality of the conclusions by extending the analysis to other supports. Finally, the findings of this study could be of help for screening studies aiming at identifying new promising candidates, but for quantitative estimates many other effects should be included in the simulation framework, such as solvation, applied voltage and pH. Further work will be dedicated to the calculation of transition state energy for the formation of unconventional intermediates on SACs to check for the existence of Bronsted-Evans-Polanyi (BEP) relationships. A recent study on Single Atom Alloys (SAAs) demonstrated that BEP relations can be broken [69].

CRediT authorship contribution statement

Ilaria Barlocco: Conceptualization, Methodology, Data curation, review and editing. **Giovanni Di Liberto:** Conceptualization, Supervision, Writing – original draft, Writing – review & editing. **Gianfranco Pacchioni:** Supervision, Funding acquisition, review and editing. The manuscript was written through contributions of all authors.

Declaration of Competing Interest

The authors declare the following financial interests/personal relationships which may be considered as potential competing interests: Gianfranco Pacchioni reports financial support was provided by Cariplo Foundation.

Data availability

Data will be made available on request.

Acknowledgements

We thank Cariplo Foundation. Access to the CINECA supercomputing resources was granted via ISCRAB. We also thank the COST Action 18234 supported by COST (European Cooperation in Science and Technology).

Appendix A. Supporting information

Supplementary data associated with this article can be found in the online version at doi:10.1016/j.cattod.2023.114409.

References

[1] B. Qiao, A. Wang, X. Yang, L.F. Allard, Z. Jiang, Y. Cui, J. Liu, J. Li, T. Zhang, Single-atom catalysis of CO oxidation using Pt1/FeOx, Nat. Chem. 3 (2011) 634–641, https://doi.org/10.1038/nchem.1095.

[2] S. Abbet, A. Sanchez, U. Heiz, W.-D. Schneider, A.M. Ferrari, G. Pacchioni, N. Rösch, Acetylene cyclotrimerization on supported size-selected Pd $_n$ clusters ($1 \leq n \leq 30$): one atom is enough!, J. Am. Chem. Soc. 122 (2000) 3453–3457, https://doi.org/10.1021/ja9922476.

[3] M.A. Bajada, J. Sanjosé-Orduna, G. Di Liberto, S. Tosoni, G. Pacchioni, T. Noël, G. Vilé, Interfacing single-atom catalysis with continuous-flow organic electrosynthesis, Chem. Soc. Rev. 51 (2022) 3898–3925, https://doi.org/10.1039/D2CS00100D.

[4] S.K. Kaiser, Z. Chen, D. Faust Akl, S. Mitchell, J. Pérez-Ramírez, Single-atom catalysts across the periodic table, Chem. Rev. 120 (2020) 11703–11809, https://doi.org/10.1021/acs.chemrev.0c00576.

[5] A. Wang, J. Li, T. Zhang, Heterogeneous single-atom catalysis, Nat. Rev. Chem. 2 (2018) 65–81, https://doi.org/10.1038/s41570-018-0010-1.

[6] D. Misra, G. Di Liberto, G. Pacchioni, CO_2 electroreduction on single atom catalysts: is water just a solvent? J. Catal. 422 (2023) 1–11, https://doi.org/10.1016/j.jcat.2023.04.002.

[7] Y. Ji, Y. Li, H. Dong, L. Ding, Y. Li, Ruthenium single-atom catalysis for electrocatalytic nitrogen reduction unveiled by grand canonical density functional theory, J. Mater. Chem. A Mater. 8 (2020) 20402–20407, https://doi.org/10.1039/D0TA06672A.

[8] G. Vilé, G. Di Liberto, S. Tosoni, A. Sivo, V. Ruta, M. Nachtegaal, A.H. Clark, S. Agnoli, Y. Zou, A. Savateev, M. Antonietti, G. Pacchioni, Azide-alkyne click chemistry over a heterogeneous copper-based single-atom catalyst, ACS Catal. 12 (2022) 2947–2958, https://doi.org/10.1021/acscatal.1c05610.

[9] N. Cheng, S. Stambula, D. Wang, M.N. Banis, J. Liu, A. Riese, B. Xiao, R. Li, T.-K. Sham, L.-M. Liu, G.A. Botton, X. Sun, Platinum single-atom and cluster catalysis of the hydrogen evolution reaction, Nat. Commun. 7 (2016), 13638, https://doi.org/10.1038/ncomms13638.

[10] C. Tang, L. Chen, H. Li, L. Li, Y. Jiao, Y. Zheng, H. Xu, K. Davey, S.-Z. Qiao, Tailoring acidic oxygen reduction selectivity on single-atom catalysts via modification of first and second coordination spheres, J. Am. Chem. Soc. 143 (2021) 7819–7827, https://doi.org/10.1021/jacs.1c03135.

[11] L. Cui, L. Cui, Z. Li, J. Zhang, H. Wang, S. Lu, Y. Xiang, A copper single-atom catalyst towards efficient and durable oxygen reduction for fuel cells, J. Mater. Chem. A Mater. 7 (2019) 16690–16695, https://doi.org/10.1039/C9TA03518D.

[12] M.K. Samantaray, V. D'Elia, E. Pump, L. Falivene, M. Harb, S. Ould Chikh, L. Cavallo, J.-M. Basset, The comparison between single atom catalysis and surface organometallic catalysis, Chem. Rev. 120 (2020) 734–813, https://doi.org/10.1021/acs.chemrev.9b00238.

[13] G.S. Parkinson, Single-atom catalysis: how structure influences catalytic performance, Catal. Lett. 149 (2019) 1137–1146, https://doi.org/10.1007/s10562-019-02709-7.

[14] F. Kraushofer, G.S. Parkinson, Single-atom catalysis: insights from model systems, Chem. Rev. 122 (2022) 14911–14939, https://doi.org/10.1021/acs.chemrev.2c00259.

[15] L. DeRita, J. Resasco, S. Dai, A. Boubnov, H.V. Thang, A.S. Hoffman, I. Ro, G. W. Graham, S.R. Bare, G. Pacchioni, X. Pan, P. Christopher, Structural evolution of

atomically dispersed Pt catalysts dictates reactivity, Nat. Mater. 18 (2019) 746–751, https://doi.org/10.1038/s41563-019-0349-9.
[16] S. Tosoni, G. Di Liberto, I. Matanovic, G. Pacchioni, Modelling single atom catalysts for water splitting and fuel cells: a tutorial review, J. Power Sources 556 (2023), 232492, https://doi.org/10.1016/j.jpowsour.2022.232492.
[17] G. Di Liberto, I. Barlocco, L. Giordano, S. Tosoni, G. Pacchioni, Single-atom electrocatalysis from first principles: current status and open challenges, Curr. Opin. Electrochem. 40 (2023), 101343, https://doi.org/10.1016/j.coelec.2023.101343.
[18] V. Fung, G. Hu, Z. Wu, D. Jiang, Descriptors for hydrogen evolution on single atom catalysts in nitrogen-doped graphene, J. Phys. Chem. C 124 (2020) 19571–19578, https://doi.org/10.1021/acs.jpcc.0c04432.
[19] H.-C. Huang, Y. Zhao, J. Wang, J. Li, J. Chen, Q. Fu, Y.-X. Bu, S.-B. Cheng, Rational design of an efficient descriptor for single-atom catalysts in the hydrogen evolution reaction, J. Mater. Chem. A Mater. 8 (2020) 9202–9208, https://doi.org/10.1039/D0TA01500H.
[20] L. Wu, T. Guo, T. Li, Rational design of transition metal single-atom electrocatalysts: a simulation-based, machine learning-accelerated study, J. Mater. Chem. A Mater. 8 (2020) 19290–19299, https://doi.org/10.1039/D0TA06207C.
[21] M.D. Hossain, Z. Liu, M. Zhuang, X. Yan, G.-L. Xu, C.A. Gadre, A. Tyagi, I.H. Abidi, C.-J. Sun, H. Wong, A. Guda, Y. Hao, X. Pan, K. Amine, Z. Luo, Rational design of graphene-supported single atom catalysts for hydrogen evolution reaction, Adv. Energy Mater. 9 (2019), 1803689, https://doi.org/10.1002/aenm.201803689.
[22] J.K. Nørskov, T. Bligaard, J. Rossmeisl, C.H. Christensen, Towards the computational design of solid catalysts, Nat. Chem. 1 (2009) 37–46, https://doi.org/10.1038/nchem.121.
[23] J. Greeley, I.E.L. Stephens, A.S. Bondarenko, T.P. Johansson, H.A. Hansen, T. F. Jaramillo, J. Rossmeisl, I. Chorkendorff, J.K. Nørskov, Alloys of platinum and early transition metals as oxygen reduction electrocatalysts, Nat. Chem. 1 (2009) 552–556, https://doi.org/10.1038/nchem.367.
[24] J.K. Nørskov, T. Bligaard, A. Logadottir, J.R. Kitchin, J.G. Chen, S. Pandelov, U. Stimming, Trends in the exchange current for hydrogen evolution, J. Electrochem. Soc. 152 (2005) J23, https://doi.org/10.1149/1.1856988.
[25] A. Kulkarni, S. Siahrostami, A. Patel, J.K. Nørskov, Understanding catalytic activity trends in the oxygen reduction reaction, Chem. Rev. 118 (2018) 2302–2312, https://doi.org/10.1021/acs.chemrev.7b00488.
[26] J.K. Nørskov, J. Rossmeisl, A. Logadottir, L. Lindqvist, J.R. Kitchin, T. Bligaard, H. Jónsson, Origin of the overpotential for oxygen reduction at a fuel-cell cathode, J. Phys. Chem. B 108 (2004) 17886–17892, https://doi.org/10.1021/jp047349j.
[27] Z.W. Seh, J. Kibsgaard, C.F. Dickens, I. Chorkendorff, J.K. Nørskov, T.F. Jaramillo, Combining theory and experiment in electrocatalysis: insights into materials design, Science (1979) 355 (2017), eaad4998, https://doi.org/10.1126/science.aad4998.
[28] E. Skúlason, G.S. Karlberg, J. Rossmeisl, T. Bligaard, J. Greeley, H. Jónsson, J. K. Nørskov, Density functional theory calculations for the hydrogen evolution reaction in an electrochemical double layer on the Pt(111) electrode, Phys. Chem. Chem. Phys. 9 (2007) 3241–3250, https://doi.org/10.1039/B700099E.
[29] I.C. Man, H. Su, F. Calle-Vallejo, H.A. Hansen, J.I. Martínez, N.G. Inoglu, J. Kitchin, T.F. Jaramillo, J.K. Nørskov, J. Rossmeisl, Universality in oxygen evolution electrocatalysis on oxide surfaces, ChemCatChem 3 (2011) 1159–1165, https://doi.org/10.1002/cctc.201000397.
[30] M.T.M. Koper, Thermodynamic theory of multi-electron transfer reactions: implications for electrocatalysis, J. Electroanal. Chem. 660 (2011) 254–260, https://doi.org/10.1016/j.jelechem.2010.10.004.
[31] N. Govindarajan, M.T.M. Koper, E.J. Meijer, F. Calle-Vallejo, Outlining the scaling-based and scaling-free optimization of electrocatalysts, ACS Catal. 9 (2019) 4218–4225, https://doi.org/10.1021/acscatal.9b00532.
[32] L. Zhong, S. Li, Unconventional oxygen reduction reaction mechanism and scaling relation on single-atom catalysts, ACS Catal. 10 (2020) 4313–4318, https://doi.org/10.1021/acscatal.0c00815.
[33] I. Barlocco, L.A. Cipriano, G. Di Liberto, G. Pacchioni, Does the oxygen evolution reaction follow the classical OH*, O*, OOH* path on single atom catalysts? J. Catal. 417 (2023) 351–359, https://doi.org/10.1016/j.jcat.2022.12.014.
[34] L. Li, K. Yuan, Y. Chen, Breaking the scaling relationship limit: from single-atom to dual-atom catalysts, Acc. Mater. Res. 3 (2022) 584–596, https://doi.org/10.1021/accountsmr.1c00264.
[35] Y. Ouyang, L. Shi, X. Bai, Q. Li, J. Wang, Breaking scaling relations for efficient CO $_2$ electrochemical reduction through dual-atom catalysts, Chem. Sci. 11 (2020) 1807–1813, https://doi.org/10.1039/C9SC05236D.
[36] J. Wang, Z. Zhang, Y. Li, Y. Qu, Y. Li, W. Li, M. Zhao, Screening oF Transition-metal Single-atom Catalysts Anchored on Covalent–organic Frameworks for efficient nitrogen fixation, ACS Appl. Mater. Interfaces 14 (2022) 1024–1033, https://doi.org/10.1021/acsami.1c20373.
[37] G. Kresse, J. Hafner, Ab initio molecular dynamics for liquid metals, Phys. Rev. B 47 (1993) 558–561, https://doi.org/10.1103/PhysRevB.47.558.
[38] G. Kresse, J. Furthmüller, Efficiency of ab-initio total energy calculations for metals and semiconductors using a plane-wave basis set, Comput. Mater. Sci. 6 (1996) 15–50, https://doi.org/10.1016/0927-0256(96)00008-0.
[39] G. Kresse, J. Hafner, Ab initio molecular-dynamics simulation of the liquid-metal–amorphous-semiconductor transition in germanium, Phys. Rev. B 49 (1994) 14251–14269, https://doi.org/10.1103/PhysRevB.49.14251.
[40] J.P. Perdew, K. Burke, M. Ernzerhof, Generalized gradient approximation made simple, Phys. Rev. Lett. 77 (1996) 3865–3868, https://doi.org/10.1103/PhysRevLett.77.3865.
[41] P.E. Blöchl, Projector augmented-wave method, Phys. Rev. B 50 (1994) 17953–17979, https://doi.org/10.1103/PhysRevB.50.17953.
[42] G. Kresse, D. Joubert, From ultrasoft pseudopotentials to the projector augmented-wave method, Phys. Rev. B 59 (1999) 1758–1775, https://doi.org/10.1103/PhysRevB.59.1758.
[43] S. Grimme, J. Antony, S. Ehrlich, H. Krieg, A consistent and accurate ab initio parametrization of density functional dispersion correction (DFT-D) for the 94 elements H-Pu, J. Chem. Phys. 132 (2010), 154104, https://doi.org/10.1063/1.3382344.
[44] A.M. Patel, S. Ringe, S. Siahrostami, M. Bajdich, J.K. Nørskov, A.R. Kulkarni, Theoretical approaches to describing the oxygen reduction reaction activity of single-atom catalysts, J. Phys. Chem. C 122 (2018) 29307–29318, https://doi.org/10.1021/acs.jpcc.8b09430.
[45] G. Di Liberto, L.A. Cipriano, G. Pacchioni, Universal principles for the rational design of single atom electrocatalysts? Handle with care, ACS Catal. (2022) 5846–5856, https://doi.org/10.1021/acscatal.2c01011.
[46] I. Barlocco, L.A. Cipriano, G. Di Liberto, G. Pacchioni, Modeling Hydrogen and Oxygen Evolution Reactions on Single Atom Catalysts with Density Functional Theory: Role of the Functional, Adv. Theory Simul. (2022), 2200513, https://doi.org/10.1002/adts.202200513.
[47] H. Fei, J. Dong, M.J. Arellano-Jiménez, G. Ye, N. Dong Kim, E.L.G. Samuel, Z. Peng, Z. Zhu, F. Qin, J. Bao, M.J. Yacaman, P.M. Ajayan, D. Chen, J.M. Tour, Atomic cobalt on nitrogen-doped graphene for hydrogen generation, Nat. Commun. 6 (2015), 8668, https://doi.org/10.1038/ncomms9668.
[48] D. Van Dao, L.A. Cipriano, G. Di Liberto, T.T.D. Nguyen, S.-W. Ki, H. Son, G.-C. Kim, K.H. Lee, J.-K. Yang, Y.-T. Yu, G. Pacchioni, I.-H. Lee, Plasmonic Au nanoclusters dispersed in nitrogen-doped graphene as a robust photocatalyst for light-to-hydrogen conversion, J. Mater. Chem. A Mater. 9 (2021) 22810–22819, https://doi.org/10.1039/D1TA05445G.
[49] D. Van Dao, G. Di Liberto, H. Ko, J. Park, W. Wang, D. Shin, H. Son, Q. Van Le, T. Van Nguyen, V. Van Tan, G. Pacchioni, I.-H. Lee, LaFeO 3 meets nitrogen-doped graphene functionalized with ultralow Pt loading in an impactful Z-scheme platform for photocatalytic hydrogen evolution, J. Mater. Chem. A Mater. 10 (2022) 3330–3340, https://doi.org/10.1039/D1TA10376H.
[50] V. Hasija, S. Patial, P. Raizada, A. Aslam Parwaz Khan, A.M. Asiri, Q. Van Le, V.-H. Nguyen, P. Singh, Covalent organic frameworks promoted single metal atom catalysis: strategies and applications, Coord. Chem. Rev. 452 (2022), 214298, https://doi.org/10.1016/j.ccr.2021.214298.
[51] M. Lu, M. Zhang, C. Liu, J. Liu, L. Shang, M. Wang, J. Chang, S. Li, Y. Lan, Stable dioxin-linked metallophthalocyanine covalent organic frameworks (COFs) as photo-coupled electrocatalysts for CO $_2$ reduction, Angew. Chem. 133 (2021) 4914–4921, https://doi.org/10.1002/ange.202011722.
[52] C. Lin, L. Zhang, Z. Zhao, Z. Xia, Design principles for covalent organic frameworks as efficient electrocatalysts in clean energy conversion and green oxidizer production, Adv. Mater. 29 (2017), 1606635, https://doi.org/10.1002/adma.201606635.
[53] L.A. Cipriano, G. Di Liberto, G. Pacchioni, Superoxo and Peroxo complexes on single-atom catalysts: impact on the oxygen evolution reaction, ACS Catal. (2022) 11682–11691, https://doi.org/10.1021/acscatal.2c03020.
[54] G. Pacchioni, Modeling doped and defective oxides in catalysis with density functional theory methods: room for improvements, J. Chem. Phys. 128 (2008), https://doi.org/10.1063/1.2819245.
[55] E. Sargeant, F. Illas, P. Rodríguez, F. Calle-Vallejo, Importance of the gas-phase error correction for O2 when using DFT to model the oxygen reduction and evolution reactions, J. Electroanal. Chem. 896 (2021), 115178, https://doi.org/10.1016/j.jelechem.2021.115178.
[56] I. Barlocco, G. Di Liberto, G. Pacchioni, Hydrogen and oxygen evolution reactions on single atom catalysts stabilized by a covalent organic framework, Energy Adv. (2023), https://doi.org/10.1039/D3YA00162H.
[57] M.T. Greiner, T.E. Jones, S. Beeg, L. Zwiener, M. Scherzer, F. Girgsdies, S. Piccinin, M. Armbrüster, A. Knop-Gericke, R. Schlögl, Free-atom-like d states in single-atom alloy catalysts, Nat. Chem. 10 (2018) 1008–1015, https://doi.org/10.1038/s41557-018-0125-5.
[58] J. Koseki, R. Maezono, M. Tachikawa, M.D. Towler, R.J. Needs, Quantum Monte Carlo study of porphyrin transition metal complexes, J. Chem. Phys. 129 (2008), https://doi.org/10.1063/1.2966003.
[59] A. Garai, M. Villa, M. Marchini, S.K. Patra, T. Pain, S. Mondal, P. Ceroni, S. Kar, Synthesis, structure, photophysics, and singlet oxygen sensitization by a platinum (II) complex of meso -tetra-acenaphthyl porphyrin, Eur. J. Inorg. Chem. 2021 (2021) 4089–4095, https://doi.org/10.1002/ejic.202100667.
[60] S. Hong, K.D. Sutherlin, J. Park, E. Kwon, M.A. Siegler, E.I. Solomon, W. Nam, Crystallographic and spectroscopic characterization and reactivities of a mononuclear non-haem iron(III)-superoxo complex, Nat. Commun. 5 (2014), 5440, https://doi.org/10.1038/ncomms6440.
[61] M.R. Anneser, S. Haslinger, A. Pöthig, M. Cokoja, V. D'Elia, M.P. Högerl, J.-M. Basset, F.E. Kühn, Binding of molecular oxygen by an artificial heme analogue: investigation on the formation of an Fe–tetracarbene superoxo complex, Dalton Trans. 45 (2016) 6449–6455, https://doi.org/10.1039/C6DT00538A.
[62] F.E. Kühn, A.M. Santos, M. Abrantes, Mononuclear organomolybdenum(VI) dioxo complexes: synthesis, reactivity, and catalytic applications, Chem. Rev. 106 (2006) 2455–2475, https://doi.org/10.1021/cr040703p.
[63] J.J. Kennedy-Smith, K.A. Nolin, H.P. Gunterman, F.D. Toste, Reversing the role of the metal−oxygen π-bond. chemoselective catalytic reductions with a rhenium(V)-dioxo complex, J. Am. Chem. Soc. 125 (2003) 4056–4057, https://doi.org/10.1021/ja029498q.
[64] J.K. Nørskov, T. Bligaard, A. Logadottir, S. Bahn, L.B. Hansen, M. Bollinger, H. Bengaard, B. Hammer, Z. Sljivancanin, M. Mavrikakis, Y. Xu, S. Dahl, C.J.

H. Jacobsen, Universality in heterogeneous catalysis, J. Catal. 209 (2002) 275–278, https://doi.org/10.1006/jcat.2002.3615.
[65] F. Calle-Vallejo, M.D. Pohl, D. Reinisch, D. Loffreda, P. Sautet, A.S. Bandarenka, Why conclusions from platinum model surfaces do not necessarily lead to enhanced nanoparticle catalysts for the oxygen reduction reaction, Chem. Sci. 8 (2017) 2283–2289, https://doi.org/10.1039/C6SC04788B.
[66] Y. Wu, C. Li, W. Liu, H. Li, Y. Gong, L. Niu, X. Liu, C. Sun, S. Xu, Unexpected monoatomic catalytic-host synergetic OER/ORR by graphitic carbon nitride: density functional theory, Nanoscale 11 (2019) 5064–5071, https://doi.org/10.1039/C8NR09300H.
[67] Y. Ying, K. Fan, X. Luo, J. Qiao, H. Huang, Unravelling the origin of bifunctional OER/ORR activity for single-atom catalysts supported on C 2 N by DFT and machine learning, J. Mater. Chem. A Mater. 9 (2021) 16860–16867, https://doi.org/10.1039/D1TA04256D.
[68] S. Lu, H.L. Huynh, F. Lou, K. Guo, Z. Yu, Single transition metal atom embedded antimonene monolayers as efficient trifunctional electrocatalysts for the HER, OER and ORR: a density functional theory study, Nanoscale 13 (2021) 12885–12895, https://doi.org/10.1039/D1NR02235K.
[69] M.T. Darby, M. Stamatakis, A. Michaelides, E.CharlesH. Sykes, Lonely atoms with special gifts: breaking linear scaling relationships in heterogeneous catalysis with single-atom alloys, J. Phys. Chem. Lett. 9 (2018) 5636–5646, https://doi.org/10.1021/acs.jpclett.8b01888.